different from the clinical symptoms of conventional mitochondrial myopathy. Thus, based on the available evidence, we believe that patients 1 and 2 can be diagnosed with mitochondrial predominant axial myopathy.

Axial myopathy may occur secondary to various diseases. However, only five cases of mitochondrial axial myopathy associated with the prominent involvement of the extensor muscles of the spine have been previously reported (Table 2) [8, 11, 28, 30, 32]. All these cases presented with abnormal trunk flexion that developed during walking and disappeared when the patient was in a supine position. In the cases described here, only patient 2 presented with camptocormia. These common symptoms, including late-onset, mildly elevated serum CK levels, ragged-red fibers, and the partial deficiency in COX activities, were observed in patient 1 and also in the above mentioned cases. However, biochemical analysis was performed in only one case that showed deficiencies in complexes I and III [32]. No case has been previously reported that describes a family history of similar symptoms. In addition, no genetic cause of any mitochondrial axial myopathy has been previously reported.

This study is unable to conclusively prove or disprove the pathogenicity of the m.602C>T mutation. However, three reasons that support the pathogenicity of this mutation are apparent. First, the heteroplasmic m.602C>T point mutation disrupts a conserved Watson–Crick cytosine–guanine (C–G) base pairing within the D-stem of the mitochondrial tRNA[Phe] gene, which would most likely affect the stability of the secondary structure of mitochondrial tRNA (Fig. 5b). Almost 94% of mitochondrial tRNA pathogenic mutations occur in this stem structure, and the disruption of Watson–Crick C–G base pairing is a significantly more common feature of pathogenic mutations than neutral variants [23]. Second, after performing a sequence homology search using CLUSTALW (http://clustalw. ddbj.nig.ac.jp/top-j.html), it was determined that this base pairing is largely conserved in other species as C–G or adenine–thymine base pairings (Fig. 5c). Third, the

mutation is heteroplasmic and present in the affected skeletal muscles but not in the peripheral blood lymphocytes. Almost all pathogenic mitochondrial tRNA mutations in clinically affected tissues have a high proportion of heteroplasmy compared with unaffected tissues [23].

However, the decreased activities of complexes I and IV that were observed during the biochemical examination cannot be completely explained by the disruption in mitochondrial protein synthesis that could have been caused by the mitochondrial tRNA mutation. In addition, data obtained from the single muscle fiber analyses were limited due to the small sample size, and therefore, are not sufficient to prove the pathogenicity of the m.602C>T mutation.

Any additional evidence of the pathogenicity of the cybrid cells was not obtained. Therefore, 10 points (out of a maximum score of 20 points) was applied to the scoring criteria of the mitochondrial tRNA mutations listed in MITOMAP, which indicated that the m.602C>T mutation is possibly pathogenic [23].

The mechanism of late-onset axial myopathy induced by mitochondrial dysfunction is unclear. Nine pathogenic mutations in the mitochondrial tRNA[Phe] gene have been previously described in various diseases (Fig. 5b), including a late-onset neuromuscular disease but not axial myopathy [7, 9, 12, 14, 17, 18, 22, 25, 34, 35]. A probable etiological mechanism for the presentation of such a myopathy in the elderly is the accumulation of mitochondrial tRNA pathogenic mutations that affect aging tissues [9]. If it is possible to get any information on the pathological status of the primarily affected muscles, this would perhaps be as informative as the differential involvement of the biceps and paraspinal muscles. Unfortunately, these data could not be obtained due to the remarkable fatty degeneration of the paraspinal muscles.

The patients described in this report are characterized by the combination of axial myopathy and CNS involvement. One report about a parkinsonian patient with mitochondrial axial myopathy suggested that mitochondrial dysfunction

Table 2 Clinical characteristics of patients with paraspinal muscle atrophy from mitochondrial myopathy

Age/sex [Ref.]	Onset age	Family history	CK (IU/l)	RRF	COX deficiency	mtDNA mutation	Neurological deficit
73/F [patient 1]	63	+	290	+	+	602C>T	Cerebellar ataxia
84/F [patient 2]	60	+	474	NE	NE	NE	Encephalopathy
65/M [32]	59	−	245	+	+	NR	−
65/M [30]	62	NR	NR	+	+	NR	Parkinsonism
78/M [11]	78	NR	501	+	+	NR	−
64/M [28]	NR	NR	Elevated	+	+	NR	−
55/M [8]	NR	NR	Normal	+	+	NR	−

M male, *F* female, *CK* creatine kinase, *RRF* ragged-red fiber, *NR* not reported, *NE* not evaluated, *COX* cytochrome *c* oxidase, *mtDNA* mitochondrial DNA, *Ref* reference

may lead to both axial myopathy and parkinsonism [30]. In the patients described here, CNS involvement was similar to that observed in myoclonus epilepsy with ragged-red fiber (MERRF) due to the accompanying cerebellar atrophy and epilepsy. In fact, MERRF has been previously reported to be associated with pathogenic mutations of the mitochondrial tRNA^{Phe} gene [22].

Finally, mitochondrial dysfunction might be implicated in the development of Hashimoto thyroiditis in patients 1 and 2 and in the fourth son of patient 2; the relationship between mitochondrial diseases and Hashimoto thyroiditis has been previously described [3, 20, 26, 27].

In summary, this is the first report about familial mitochondrial disease with late-onset predominant axial myopathy and encephalopathy, which were confirmed by clinical and histological findings. This case expands the phenotypic spectrum of mitochondrial diseases. Future studies on the novel mitochondrial tRNA^{Phe} 602C>T mutation may contribute to the understanding of late-onset predominant axial myopathy and encephalopathy.

References

1. Azher SN, Jankovic J (2005) Camptocormia: pathogenesis, classification, and response to therapy. Neurology 65:355–359
2. Bai RK, Wong LJ (2004) Detection and quantification of heteroplasmic mutant mitochondrial DNA by real-time amplification refractory mutation system quantitative PCR analysis: a single-step approach. Clin Chem 50:996–1001
3. Berio A, Piazzi A (2002) A case of Kearns-Sayre syndrome with autoimmune thyroiditis and possible Hashimoto encephalopathy. Panminerva Med 44:265–269
4. Bernier FP, Boneh A, Dennett X, Chow CW, Cleary MA, Thorburn DR (2002) Diagnostic criteria for respiratory chain disorders in adults and children. Neurology 59:1406–1411
5. Boerkoel CF, Takashima H, Stankiewicz P et al (2001) Periaxin mutations cause recessive Dejerine-Sottas neuropathy. Am J Hum Genet 68:325–333
6. D'Aurelio M, Gajewski CD, Lenaz G, Manfredi G (2006) Respiratory chain supercomplexes set the threshold for respiration defects in human mtDNA mutant cybrids. Hum Mol Genet 15:2157–2169
7. Darin N, Kollberg G, Moslemi AR et al (2006) Mitochondrial myopathy with exercise intolerance and retinal dystrophy in a sporadic patient with a G583A mutation in the mt tRNA(phe) gene. Neuromuscul Disord 16:504–506
8. Delcey V, Hachulla E, Michon-Pasturel U et al (2002) Camptocormia: a sign of axial myopathy. Report of 7 cases. Rev Med Interne 23:144–154
9. Deschauer M, Swalwell H, Strauss M, Zierz S, Taylor RW (2006) Novel mitochondrial transfer RNA(Phe) gene mutation associated with late-onset neuromuscular disease. Arch Neurol 63:902–905
10. Genasetti A, Valentino ML, Carelli V et al (2007) Assessing heteroplasmic load in Leber's hereditary optic neuropathy mutation 3460G->A/MT-ND1 with a real-time PCR quantitative approach. J Mol Diagn 9:538–545
11. Gomez-Puerta JA, Peris P, Grau JM, Martinez MA, Guanabens N (2007) Camptocormia as a clinical manifestation of mitochondrial myopathy. Clin Rheumatol 26:1017–1019
12. Hanna MG, Nelson IP, Morgan-Hughes JA, Wood NW (1998) MELAS: a new disease associated mitochondrial DNA mutation and evidence for further genetic heterogeneity. J Neurol Neurosurg Psychiatry 65:512–517
13. Higuchi I, Niiyama T, Uchida Y et al (1999) Multiple episodes of thrombosis in a patient with Becker muscular dystrophy with marked expression of utrophin on the muscle cell membrane. Acta Neuropathol 98:313–316
14. Iizuka T, Goto Y, Miyakawa S et al (2009) Progressive carotid artery stenosis with a novel tRNA phenylalanine mitochondrial DNA mutation. J Neurol Sci 278:35–40
15. Jungbluth H, Lillis S, Zhou H et al (2009) Late-onset axial myopathy with cores due to a novel heterozygous dominant mutation in the skeletal muscle ryanodine receptor (RYR1) gene. Neuromuscul Disord 19:344–347
16. Karbowski K (1999) The old and the new camptocormia. Spine (Phila Pa 1976) 24:1494–1498
17. Kleinle S, Schneider V, Moosmann P, Brandner S, Krahenbuhl S, Liechti-Gallati S (1998) A novel mitochondrial tRNA(Phe) mutation inhibiting anticodon stem formation associated with a muscle disease. Biochem Biophys Res Commun 247:112–115
18. Konings A, Van Camp G, Goethals A et al (2008) Mutation analysis of mitochondrial DNA 12SrRNA and tRNASer(UCN) genes in non-syndromic hearing loss patients. Mitochondrion 8:377–382
19. Kottlors M, Kress W, Meng G, Glocker FX (2010) Facioscapulohumeral muscular dystrophy presenting with isolated axial myopathy and bent spine syndrome. Muscle Nerve 42:273–275
20. Kovacs GG, Hoftberger R, Majtenyi K et al (2005) Neuropathology of white matter disease in Leber's hereditary optic neuropathy. Brain 128:35–41
21. Mahjneh I, Marconi G, Paetau A, Saarinen A, Salmi T, Somer H (2002) Axial myopathy–an unrecognised entity. J Neurol 249:730–734
22. Mancuso M, Filosto M, Mootha VK et al (2004) A novel mitochondrial tRNAPhe mutation causes MERRF syndrome. Neurology 62:2119–2121
23. McFarland R, Elson JL, Taylor RW, Howell N, Turnbull DM (2004) Assigning pathogenicity to mitochondrial tRNA mutations: when "definitely maybe" is not good enough. Trends Genet 20:591–596
24. Mithani SK, Smith IM, Zhou S et al (2007) Mitochondrial resequencing arrays detect tumor-specific mutations in salivary rinses of patients with head and neck cancer. Clin Cancer Res 13:7335–7340
25. Moslemi AR, Lindberg C, Toft J, Holme E, Kollberg G, Oldfors A (2004) A novel mutation in the mitochondrial tRNA(Phe) gene

associated with mitochondrial myopathy. Neuromuscul Disord 14:46–50

26. Muller-Hocker J, Jacob U, Seibel P (1998) Hashimoto thyroiditis is associated with defects of cytochrome-c oxidase in oxyphil Askanazy cells and with the common deletion (4, 977) of mitochondrial DNA. Ultrastruct Pathol 22:91–100

27. Ohno K, Yamamoto M, Engel AG et al (1996) MELAS- and Kearns-Sayre-type co-mutation [corrected] with myopathy and autoimmune polyendocrinopathy. Ann Neurol 39:761–766

28. Poullin P, Daumen-Legre V, Serratrice G (1993) Camptocormia in the elderly patient: myopathy or muscular dystonia? Rev Rhum Ed Fr 60:159–161

29. Rieder MJ, Taylor SL, Tobe VO, Nickerson DA (1998) Automating the identification of DNA variations using quality-based fluorescence re-sequencing: analysis of the human mitochondrial genome. Nucleic Acids Res 26:967–973

30. Schabitz WR, Glatz K, Schuhan C et al (2003) Severe forward flexion of the trunk in Parkinson's disease: focal myopathy of the paraspinal muscles mimicking camptocormia. Mov Disord 18:408–414

31. Serratrice G (2007) Axial myopathies: an elderly disorder. Acta Myol 26:11–13

32. Serratrice G, Pouget J, Pellissier JF (1996) Bent spine syndrome. J Neurol Neurosurg Psychiatry 60:51–54

33. Trounce IA, Kim YL, Jun AS, Wallace DC (1996) Assessment of mitochondrial oxidative phosphorylation in patient muscle biopsies, lymphoblasts, and transmitochondrial cell lines. Methods Enzymol 264:484–509

34. Tzen CY, Tsai JD, Wu TY et al (2001) Tubulointerstitial nephritis associated with a novel mitochondrial point mutation. Kidney Int 59:846–854

35. Valente L, Piga D, Lamantea E et al (2009) Identification of novel mutations in five patients with mitochondrial encephalomyopathy. Biochim Biophys Acta 1787:491–501

36. Wittig I, Braun HP, Schagger H (2006) Blue native PAGE. Nat Protoc 1:418–428

37. Zhou S, Kassauei K, Cutler DJ et al (2006) An oligonucleotide microarray for high-throughput sequencing of the mitochondrial genome. J Mol Diagn 8:476–482

ORIGINAL ARTICLE

Morphological Progression of Myelin Abnormalities in IgM-Monoclonal Gammopathy of Undetermined Significance Anti–Myelin-Associated Glycoprotein Neuropathy

Yuichi Kawagashira, MD, Haruki Koike, MD, PhD, Minoru Tomita, MD, Saori Morozumi, MD, Masahiro Iijima, MD, PhD, Tomohiko Nakamura, MD, PhD, Masahisa Katsuno, MD, PhD, Fumiaki Tanaka, MD, PhD, and Gen Sobue, MD, PhD

Abstract

To characterize the morphological progression of neuropathy associated with immunoglobulin M–monoclonal gammopathy of undetermined significance with anti–myelin-associated glycoprotein antibody, we assessed histopathologic features of sural nerve specimens from 15 patients, emphasizing widely spaced myelin (WSM), demyelination, and tomaculous changes. The frequency of WSM correlated with that of demyelination and tomaculous appearance in teased-fiber preparations. In longitudinal sections at nodes of Ranvier and paranodal regions, the spaces between terminal myelin loops, particularly those adjacent to the node of Ranvier, were widened, indicating an early change before demyelination, and there was concomitant swelling of terminal myelin loops. Some conspicuously swollen terminal myelin loops were detached from the paranodal axolemma, thereby widening the nodes of Ranvier. Tomacula coexisted frequently with redundant myelin loops and WSM, particularly in the outermost layer of myelin sheaths, suggesting that loosening of the outer layers contributes to their formation. By immunofluorescence microscopy, immunoglobulin M and myelin-associated glycoprotein were colocalized in paranodal regions and Schmidt-Lanterman incisures. Confocal analysis revealed colocalization of immunoglobulin M and complement product C3d corresponding to the area of WSM. Thus, morphological changes in terminal myelin loops, formation of WSM at paranodes, and subsequent dissociation from paranodal axolemma (which may be associated with activation of the complement pathway) likely contribute to demyelination in this condition. Loosening of compact myelin seems to contribute to tomacula formation.

Key Words: Anti-MAG antibody, IgM monoclonal gammopathy of undetermined significance, Neuropathy, Widely spaced myelin.

INTRODUCTION

Polyneuropathy associated with immunoglobulin M (IgM) monoclonal gammopathy of undetermined significance (MGUS) with anti–myelin-associated glycoprotein (MAG) antibody is characterized by late age of onset, slow progression, and sensory-motor symptoms, particularly sensory ataxia caused by predominant impairment of large myelinated nerve fibers (1–6). In a recent study, anti-MAG antibody was found in approximately 70% of patients with neuropathy-associated IgM monoclonal gammopathy (7). Much of the MAG molecule is exposed on the membrane surface and would, therefore, be an accessible antigen. A pathogenetic role for anti-MAG antibody in this neuropathy has been indicated in several studies (8–14).

Pathological studies of IgM-MGUS anti-MAG neuropathy have demonstrated the presence of IgM antibody deposits at sites of MAG localization with loss of myelinated fibers, and teased-fiber preparations have demonstrated segmental demyelination, tomaculous appearance, and axonal degeneration (3, 8, 15–20). Ultrastructural studies have shown that widely spaced myelin (WSM), in which the distance between intraperiod lines is increased, is a nearly specific finding in this condition (11, 21–25). However, it is still unclear whether WSM is caused by the deposition of IgM antibody and how WSM relates to the onset of demyelination or tomacula. Furthermore, the morphological changes that occur during demyelination in this neuropathy, particularly where demyelination begins, what the earliest change is, and how demyelination may affect axonal structure are not known.

This study demonstrated morphological features of demyelination that are unique to IgM-MGUS anti-MAG neuropathy, focusing in particular on the correlation between WSM and the process of myelin alterations, including demyelination and tomaculous formation.

MATERIALS AND METHODS

Patients

Fifteen patients with anti-MAG neuropathy who were referred to the Department of Neurology of Nagoya University Hospital and who underwent sural nerve biopsy from 1996 to 2008 were investigated. We excluded patients who had evidence of a hematologic malignancy (multiple myeloma, Waldenstrom macroglobulinemia, lymphoma, or amyloidosis) or other diseases that may have contributed to their neuropathy. Determination of MAG autoantibody titer was performed by ELISA using purified human MAG antigen (Athena Diagnostics, Worcester, MA). Confirmation of all positive MAG

ELISA tests was performed by Western blot analysis (15, 26). All patients underwent a full neurological evaluation, routine blood and urine studies, cranial magnetic resonance imaging or computed tomography, and nerve conduction studies. The clinical features and laboratory data are summarized in Table 1.

Pathological Assessment of Sural Nerve Biopsy Specimens

Sural nerve biopsy was performed before the initiation of treatment in all patients, as previously described (27–29). Specimens were divided into 2 portions. The first was fixed in 2.5% glutaraldehyde in 0.125 mol/L cacodylate buffer (pH 7.4) and embedded in epoxy resin for morphometric and ultrastructural studies. The density of myelinated fibers was assessed in toluidine blue-stained semithin sections using a computer-assisted image analyzer (Luzex FS; Nikon, Tokyo, Japan). The densities of small and large myelinated fibers were calculated as previously described (27, 28). The remainder of the glutaraldehyde-fixed sample was processed for the teased-fiber study, in which at least 200 single fibers were isolated and analyzed as described (27, 30). The second portion of each specimen was fixed in 10% formalin and embedded in paraffin. Sections were cut by routine methods and stained with hematoxylin and eosin, Congo red, the Klüver-Barrera method, and the Masson trichrome method.

For electron microscopy (EM), epoxy resin–embedded specimens were cut into 70-nm ultrathin transverse and longitudinal sections. Ultrathin sections were contrasted by staining with uranyl acetate and lead citrate. Sections were viewed with a transmission electron microscope (H-7100; Hitachi). To assess the density of unmyelinated fibers, random EM photographs were taken at a magnification of 4,000× to cover the area of the ultrathin sections, as previously described (27, 28, 31). Fibers with WSM and structures of paranodal regions and Schmidt-Lanterman incisures in longitudinal sections were confirmed in more highly magnified photographs.

Because the endoneurial area is often enlarged in patients with anti-MAG neuropathy, we evaluated the total number of sural nerve fibers as well as their densities (32). The total endoneurial area was assessed using an image analyzer (Luzex FS) when complete transverse sections of the sural nerve were obtained. To determine the total population per sural nerve cross section, the density was multiplied by the total endoneurial area from which the subperineurial space was subtracted. We obtained complete transverse sections of the sural nerve in 10 of the 15 patients and analyzed the total population per cross section in these patients.

Control samples were obtained from 5 age-matched patients who had no neurological diseases (4 men and 1 woman; age range, 66–76 years; mean ± SD, 72.4 ± 4.2 years). Specimens were processed in the same manner as for the patients with anti-MAG neuropathy.

Widely Spaced Myelin

Widely spaced myelin is defined as an increase in the distance separating the intraperiod line. The criteria for WSM are one or more wraps of myelin with a regularly separated intraperiod line and an intact major dense line occurring at the outer or inner aspect of the myelin sheath or throughout its thickness. Uncompacted myelin, which separates major dense lines with or without separation of the intraperiod line, was excluded (33). At least 300 fibers were assessed to determine the frequency of WSM in the myelinated fibers.

Assessment of Neurofilaments

To evaluate the axonal cytoskeleton of myelinated fibers, we measured the number of neurofilaments across the axon in longitudinal sections. Using EM photographs at a magnification of 50,000×, neurofilaments were counted in 1-μm widths that vertically intersected the axon. To verify the regional differences in neurofilament density, we assessed the internode, juxtaparanode, and paranode. At least 10 axons in each of these 3 regions were examined to calculate the mean number of neurofilaments in every case.

Immunostaining

Serial 7-μm-thick transverse and longitudinal cryostat sections from fresh-frozen tissue of nerve biopsy samples were incubated with the following antibodies: goat affinity-purified antibody to human IgM (5Fc μ) (1:1000; ICN/Cappel, Aurora, OH), rabbit polyclonal anti-MAG antibody (1:100; Santa Cruz Biotechnology, Santa Cruz, CA), rabbit polyclonal antibody to complement product C3d (1:400; Abcam, Cambridge, MA), or mouse anti-C5b-9 antibody (anti-terminal complement complex [anti-TCC], 1:200; Dako, Carpinteria, CA), followed by Alexa Fluor donkey anti-goat IgG (H + L, 1:1000), Alexa Fluor goat anti-rabbit IgG (H + L, 1:1000), or Alexa Fluor goat anti-mouse IgG (H + L, 1:1000). The stained sections were examined and photographed with a confocal laser scanning microscope (μ radiance BIORAD, Nikon, Tokyo, Japan).

Statistical Analyses

Quantitative patient data (mean ± SD) were compared with control values. Statistical analyses were performed using the Mann-Whitney U test, Pearson correlation coefficient analysis,
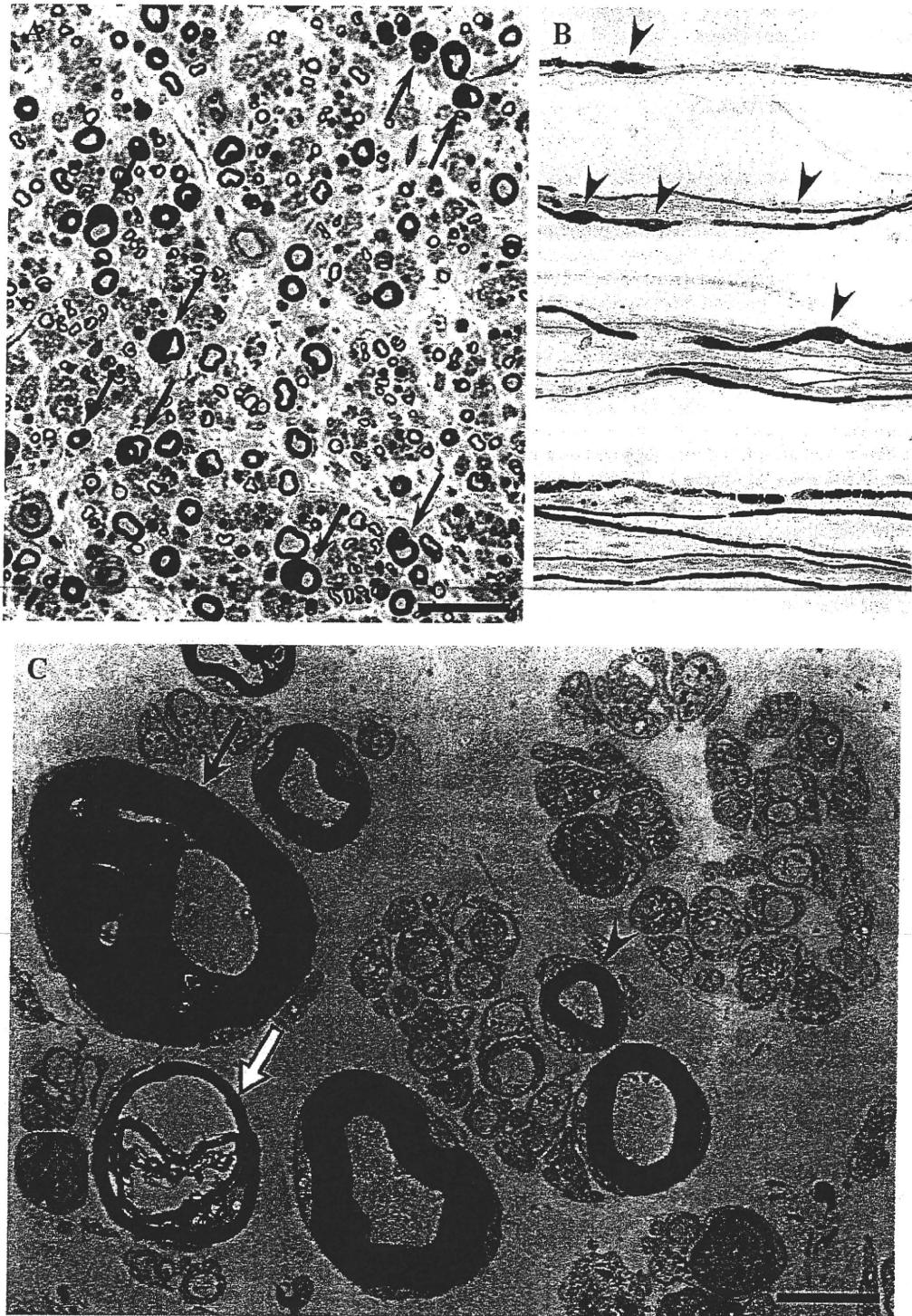
TABLE 1. Patient Characteristics

Age at examination, years	68.4 ± 7.4 (59–83)
Age at onset, years	65.8 ± 7.1 (56–82)
Sex (male/female), no.	12/3
Amount of IgM, mg/dL	697 ± 440 (244–1,794)
Light-chain kappa/lambda	13/2
CSF protein	136 ± 108 (55–381)
Nerve conduction study (mean)	
MCV, m/s; DL, ms; CMAP, mV	
Median nerve	39.2, 9.1, 6.1 (57.6, 3.4, 10.7)
Tibial nerve	29.0, 12.5, 2.2 (46.9, 4.5, 10.9)
SCV, m/s; SNAP, μV	
Median nerve	29.4, 3.6 (57.8, 23.5)
Sural nerve	37.0, 0.75 (51.0, 11.5)

Values are expressed as the number of patients, mean, or mean ± SD with the indicated ranges. Control values were obtained from 171 normal subjects and based on previously published reports.

CMAP, compound muscle action potential; CSF, cerebrospinal fluid; DL, distal latency; MCV, motor nerve conduction velocity; SCV, sensory nerve conduction velocity; SNAP, sensory nerve action potential.

FIGURE 1. Sural nerve specimens from patients with anti–myelin-associated glycoprotein neuropathy. **(A)** Transverse section shows large myelinated fibers that are markedly reduced in number compared with small myelinated fibers; some fibers show axonal atrophy and focal myelin thickening (arrows). **(B)** Teased-fiber preparation shows segmental demyelination with tomaculous appearances (arrowheads) in both intermodal and paranodal regions and axonal degeneration. Fibers undergoing degeneration and remyelination are evident in the lowest section. **(C)** Electron micrograph of a transverse section. Unmyelinated nerve fibers are well preserved. There is a fiber with tomaculous appearance and axonal atrophy (arrow), axonal degeneration (white-filled arrow), and widely spaced myelin (arrowhead). Scale bars = **(A)** 20 μm; **(C)** 5 μm.

© 2010 American Association of Neuropathologists, Inc.

and Spearman regression analysis, as appropriate. Values of p < 0.05 were considered significant.

RESULTS

Light Microscopy

In semithin cross sections, myelinated fibers in IgM-MGUS anti-MAG neuropathy biopsies were decreased versus controls. Myelin sheaths often seemed inappropriately thick for the size of the axon (Fig. 1A). The total myelinated fiber densities were reduced by varying degrees (1,422–5,703 fibers/mm^2), especially in large myelinated nerve fibers (39% of the control mean of large fibers and 61% of the control mean of small fibers) (Table 2). In teased-fiber preparations, segmental demyelination/remyelination, tomaculous appearance, and axonal degeneration coexisted (Fig. 1B). The frequency of segmental demyelination/remyelination in the teased-fiber study was high (26.8% ± 9.9%), and axonal degeneration was also frequently seen (7.5% ± 4.1%) (Table 2). Tomacula, defined as myelin thickenings of more than 50% of the fiber diameter (34), and myelin irregularity were conspicuous. The frequency of fibers with tomacula was high in all patients (Table 2). Vasculitis, inflammation, and amyloid deposition in the endoneurium were not detected.

Electron Microscopy

Transverse Sections

There were many demyelinating axons and remyelinating fibers with very thin myelin sheaths. Widely spaced

myelin and tomaculous appearance with axonal atrophy were also frequent (Fig. 1C). Widely spaced myelin was observed in all patients and was preferentially located in the outer layers of the myelin sheath (Fig. 2A), whereas in some fibers, WSM involved the entire thickness of the myelin. Tomaculous appearance with redundant myelin loops and WSM frequently coexisted (Fig. 2B). Although the typical appearance of WSM consisted of several consecutive layers of separated intraperiod lines, separation of only the outermost layer with otherwise normal-appearing myelin was also found (Figs. 2C, D). There were redundant myelin loops with tomaculous appearance consisting of infolding (Fig. 2E) and outfolding (Fig. 2G). When the separation of only the outermost layer was considered, almost all redundant myelin loops were associated with WSM. Almost all fibers with tomaculous appearance also had WSM of only the outermost or a few outer layers (Figs. 2F, H).

The frequency of WSM in myelinated fibers varied from case to case (2.6%–46.8%, 12.5% ± 14.1%; Table 3) and was positively correlated with the frequency of demyelination and tomacula in the teased-fiber study (p < 0.01, r = 0.46 and p < 0.01, r = 0.52, respectively) and negatively correlated with the total myelinated fiber density (p < 0.01, r = −0.43) (Fig. 3). However, there was no correlation between the frequency of WSM and axonal degeneration in teased-fiber preparations.

In contrast to myelinated fibers, the unmyelinated fiber density was well preserved (Fig. 1C; Table 2). On the entire transverse section of the sural nerve, the number of unmyelinated fibers was almost the same as the normal control value (Table 2). Ballooning of axons, accumulation of specific organelles, and other morphological abnormalities suggesting damage to unmyelinated axons were not apparent in any case.

Longitudinal Sections

As in the transverse sections, WSM was found preferentially in the outer layers of the myelin sheath. In paranodal regions, spaces between terminal myelin loops, especially those adjacent to the node of Ranvier, were widened compared with normal myelinated fibers (Figs. 4A, B). This widening of the spaces between terminal myelin loops seemed to continue to juxtaparanodal regions (Fig. 4B). Progression of these morphological changes, especially adjacent to the node of Ranvier, seemed to lead to WSM in paranodal regions (Fig. 4C). Concomitant with this finding, some of the terminal myelin loops, especially those adjacent to the node of Ranvier, were swollen (Fig. 4D). Some swollen terminal myelin loops were detached from the paranodal axolemma and were in juxtaparanodal regions; these loops seemed to be retracted from the paranodal regions (Figs. 5A, B). This seemed to progress to widening of the node of Ranvier (i.e. demyelination) (Figs. 6A, B). Paranodal WSM, swelling of terminal myelin loops, and detachment between the terminal myelin loops and the paranodal axolemma were found in many cases (Table 3), and their frequencies seemed to correlate with the frequency of WSM in transverse sections (p < 0.01, p < 0.05, and p < 0.05, respectively). The frequency of WSM in the transverse sections also positively correlated with anti-MAG titers (p < 0.01) (Fig. 7). The degrees of pathological abnormalities in longitudinal sections (i.e. paranodal WSM, swelling of terminal myelin loops,

TABLE 2. Pathological Features in Patients With Anti–Myelin-Associated Glycoprotein Neuropathy

	Anti-MAG Neuropathy (n = 15)	Control (n = 5)	
	Mean ± SD	Mean ± SD	p*
Myelinated fiber density, no./mm^2			
Total	3,601 ± 1,109	7,175 ± 1,227	<0.005
Large	846 ± 468	2,426 ± 468	<0.005
Small	2,755 ± 860	4,749 ± 872	<0.01
Total no. of myelinated fibers, no./nerve			
Total	4,122 ± 1,615	7,481 ± 1,359	<0.005
Large	947 ± 541	2,422 ± 460	<0.005
Small	3,175 ± 1,218	5,059 ± 1,038	<0.05
Unmyelinated fiber density, no./mm^2	26,077 ± 2,507	30,468 ± 3,472	NS
Total no. of unmyelinated fibers, no./nerve	29,915 ± 4,379	31,647 ± 3,109	NS
Teased-fiber preparation, % of fibers with			
Segmental demyelination/ remyelination	26.8 ± 9.9	12.4 ± 4.8	<0.01
Axonal degeneration	7.3 ± 4.5	3.7 ± 1.8	<0.05
Tomaculous appearance	15.9 ± 19.8	0	—

Control values (mean ± SD) are based on previously published reports.
*Determined using the Mann-Whitney U test.
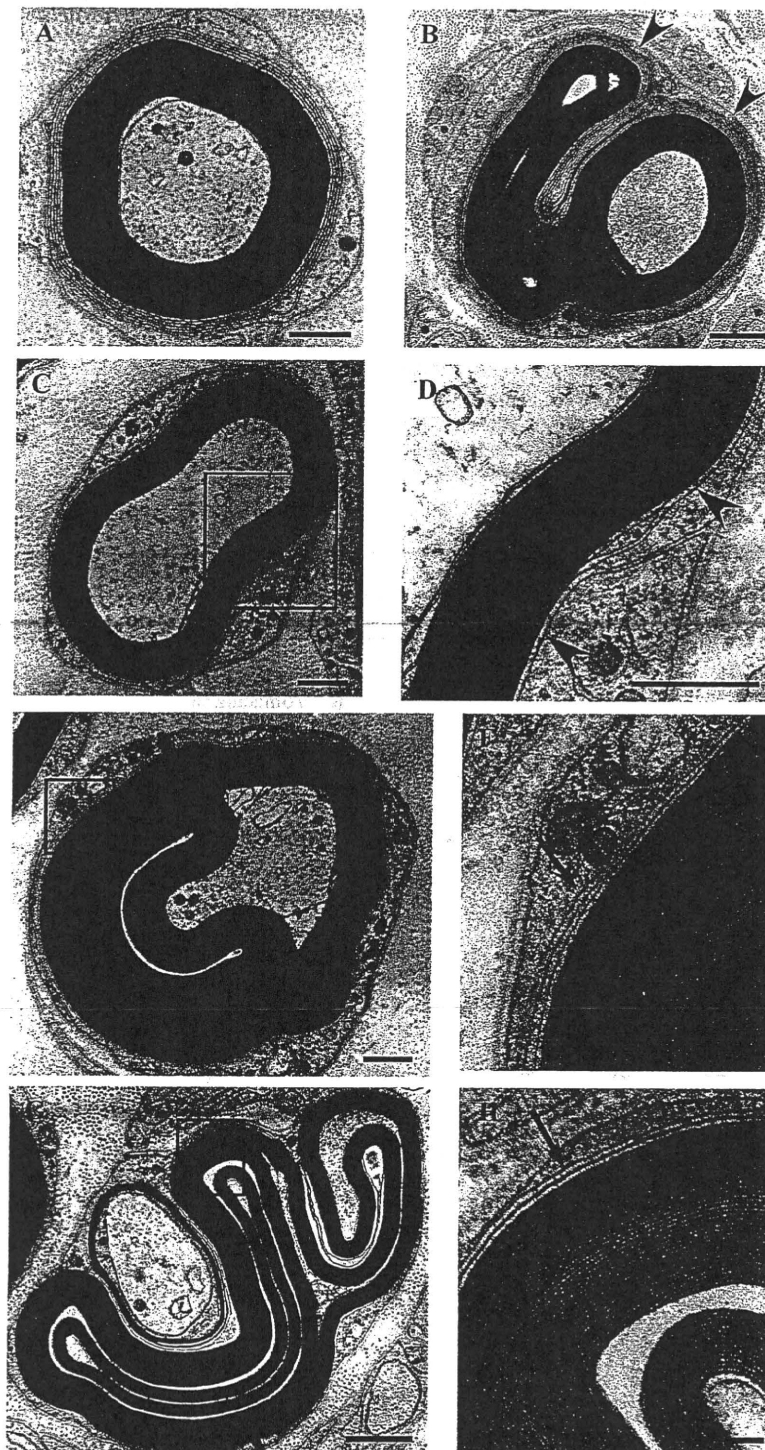MAG, myelin-associated glycoprotein; NS, not significant.

FIGURE 2. Electron micrographs of a transverse section. **(A)** Widely spaced myelin (WSM) in some outer lamellae of the myelin sheath. **(B)** Redundant myelin loops and WSM (arrowheads) in the outer layers. **(C)** Fibers with WSM in the outermost layer of the myelin sheath. **(D)** High-power micrograph of the boxed area in **(C)** shows WSM in the outermost layer in continuity with the outer mesaxon (arrowheads). **(E, G)** Redundant myelin loops with myelin infolding **(E)** and outfolding **(G)**; these features likely correspond to the tomacula seen in teased-fiber preparations. **(F, H)** High-power micrographs of the boxed areas in **(E)** and **(G)**, respectively, show WSM in the outermost or some outer layers (arrows). Scale bars = **(A–E)** 1 μm; **(F)** 0.1 μm; **(G)** 1 μm; **(H)** 0.1 μm.

TABLE 3. Pathological and Serological Data in Patients With Anti–Myelin-Associated Glycoprotein Neuropathy

Case No.	Serum IgM, mg/dL	MAG Antigen Analysis		Cross Sections			Longitudinal Sections				
		ELISA Titer	Western Blot	MF Density, no./mm²	Total No. UMF, no./nerve	Frequency of WSM, %	Swelling of TML	Paranodal WSM	Detachment Between TML and PA	SLI With WSM	Tomacula With WSM
1	379	51,200	+	2,978	28,463	9.2	+++	+	++	++	+++
2	1,794	102,400	+	1,422	—	25.3	+++	+++	+++	+++	+++
3	447	1,600	+	5,528	28,087	2.8	+	+	0	+	+
4	524	1,600	+	5,030	34,000	2.6	+	+	0	+	+
5	1,090	51,200	+	3,504	32,029	4.7	++	++	+	+	+
6	1,125	3,200	+	5,426	25,091	3.4	+	+	0	+	+
7	244	6,400	+	2,124	—	46.8	++	++	+	++	+++
8	ND	1,600	+	4,306	21,886	3.0	+	+	0	+	+
9	312	1,600	+	4,162	35,656	3.2	+	+	+	++	+
10	253	1,600	+	5,703	34,183	2.7	+	+	0	+	+
11	653	1,600	+	3,198	—	10.9	+	+	+	+	+
12	576	12,800	+	2,213	27,997	19.1	+++	+	++	+++	+
13	437	6,400	+	3,614	—	13.5	++	+	+	+	++
14	1,030	409,600	+	3,465	31,775	38.5	+++	+++	+++	+++	++
15	890	6,400	+	3,443	—	3.7	+	+	0	+	+

Lesions in nerve fibers in longitudinal sections were graded: +++ = many typical lesions; ++ = moderate number of typical lesions; + = few typical lesions; 0 = no lesions.
MAG, myelin-associated glycoprotein; MF, myelinated fiber; ND, not determined; PA, paranodal axolemma; SLI, Schmidt-Lanterman incisure; TML, terminal myelin loops; UMF, unmyelinated fiber; WSM, widely spaced myelin.
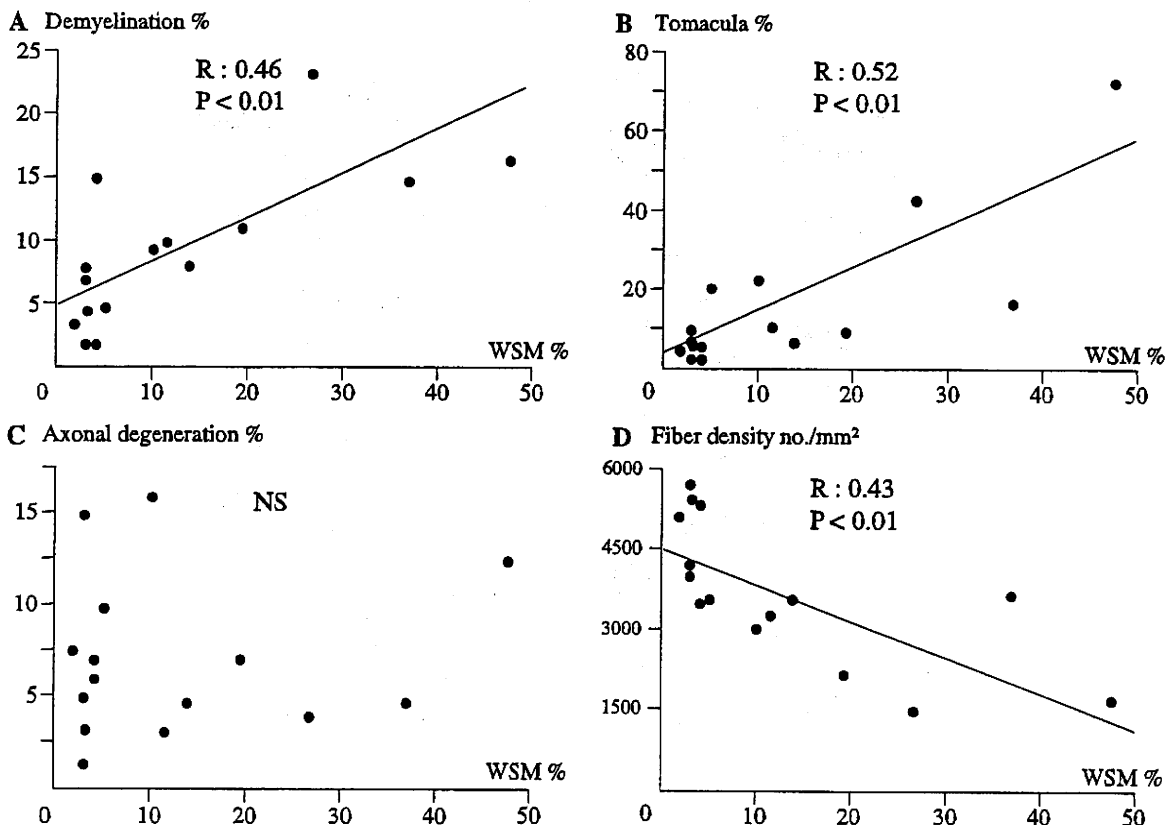

FIGURE 3. Correlations between the frequency of widely spaced myelin (WSM) and teased-fiber appearances. **(A–D)** Bold lines represent regression lines. The frequencies of demyelination **(A)**, tomacula **(B)**, and decreases in total myelinated fibers **(D)** show a positive correlation with WSM. There is no correlation between axonal degeneration and the frequency of WSM **(C)**. NS, not significant.
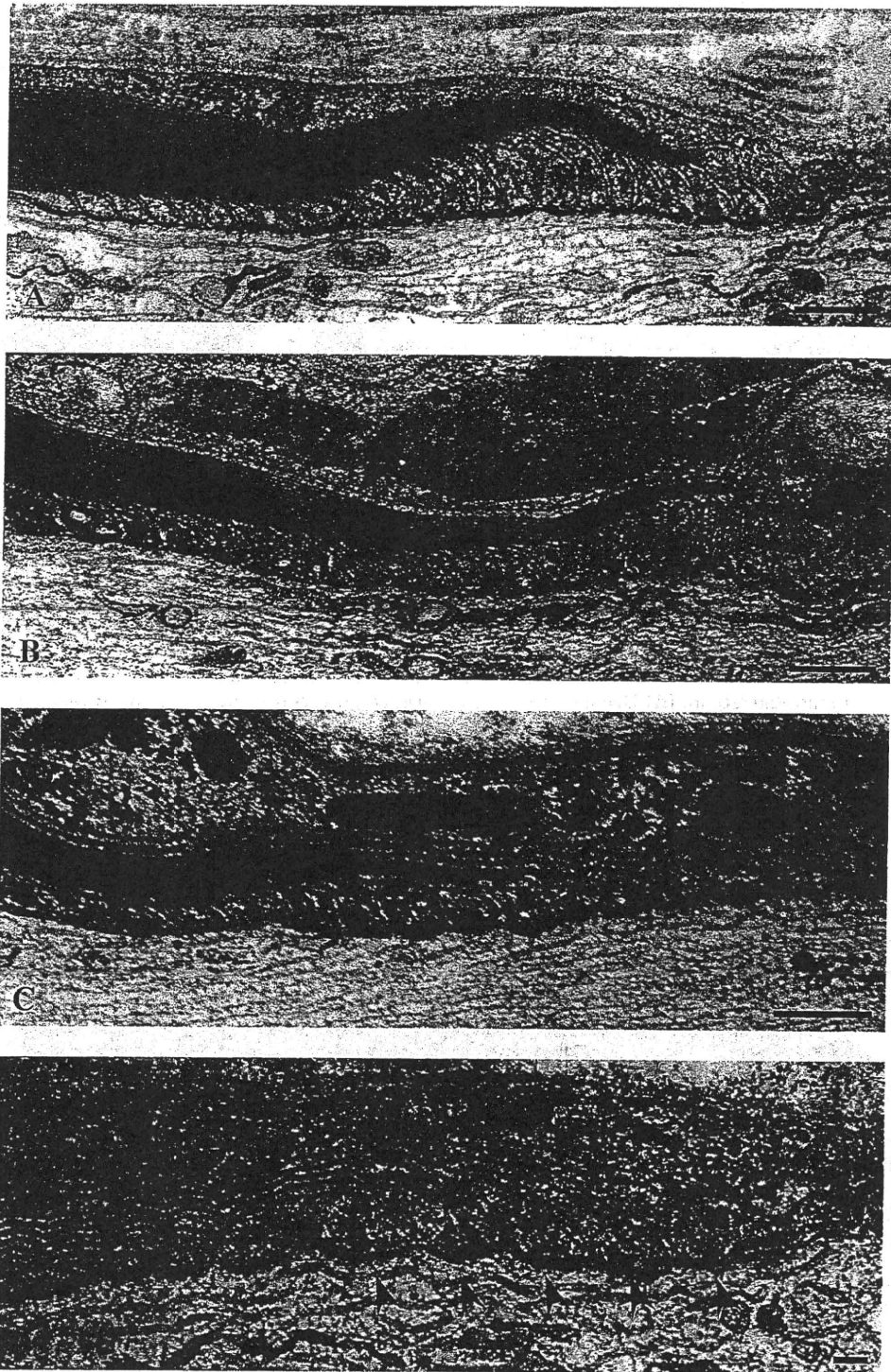
FIGURE 4. Electron micrographs of longitudinal sections in the paranodal region of nerve biopsy specimens from a normal control **(A)** and from patients with anti–myelin-associated glycoprotein neuropathy **(B–D)**. **(B)** There is widening of spaces between terminal myelin loops (arrows) that continues to the juxtaparanodal region and widely spaced myelin (WSM) in the outermost lamellae (arrowhead). **(C)** As in **(B)**, there is widening of spaces between terminal myelin loops (arrows); some outer terminal myelin loops are slightly swollen, and there is WSM in some outer layers (arrowheads). **(D)** High-power detail of terminal myelin loops adjacent to the node of Ranvier. Spaces between terminal myelin loops are widened, and outer terminal myelin loops seem swollen (arrowheads). Scale bars = **(A–C)** 0.5 μm; **(D)** 0.1 μm.
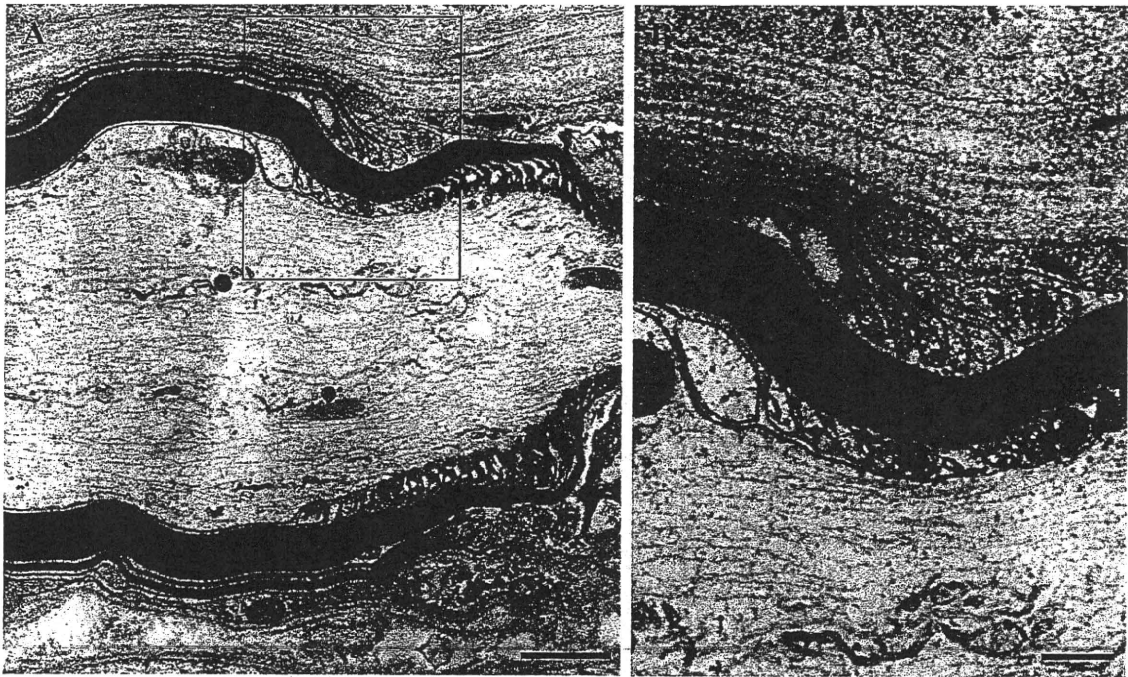
FIGURE 5. Longitudinal section from another node from a case of anti–myelin-associated glycoprotein neuropathy. **(A)** Electron micrograph shows detachment between outer terminal myelin loops and paranodal axolemma. Widely spaced myelin (WSM) is in continuity from the paranodal region. **(B)** Detail of the boxed area in **(A)** shows that outer terminal myelin loops with WSM retract from the paranodal region. Scale bars = **(A)** 0.5 μm; **(B)** 0.1 μm.
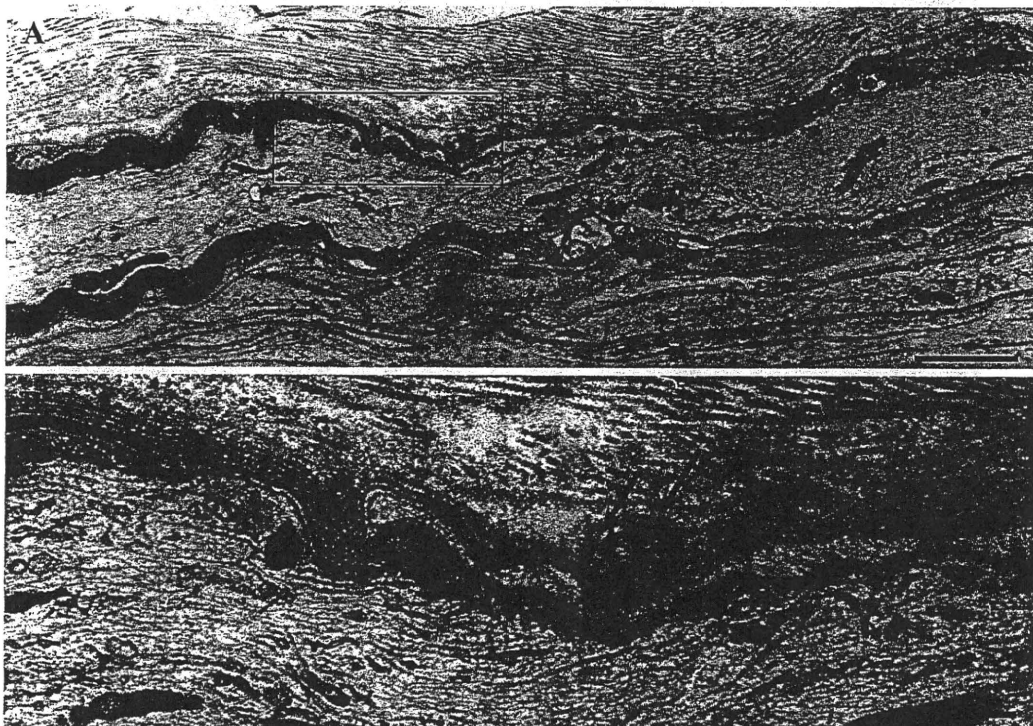

FIGURE 6. Longitudinal section from a case of anti–myelin-associated glycoprotein neuropathy. **(A)** Electron micrograph shows extensive demyelination. **(B)** Detail of the boxed area in **(A)** shows 2 terminal myelin loops that are dissociated from the paranodal axolemma (arrows). Scale bars = **(A)** 1 μm; **(B)** 0.5 μm.

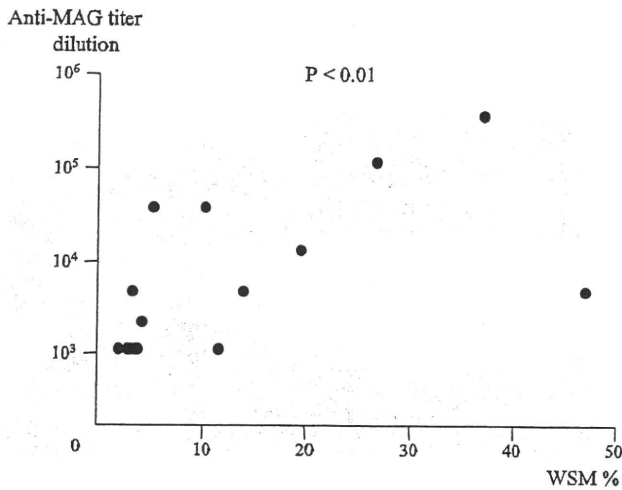1150

Anti-MAG titer dilution

FIGURE 7. Correlation between anti–myelin-associated glycoprotein (MAG) titers and frequency of widely spaced myelin (WSM) in transverse sections. The frequency of WSM in transverse sections is positively correlated with anti-MAG titers ($p < 0.01$, Spearman rank correlation analysis).

and tomacula with WSM) were also correlated with anti-MAG titers ($p < 0.05$, $p < 0.005$, and $p < 0.05$, respectively). On the other hand, serum IgM levels did not correlate with either anti-MAG titers or pathological indices (Table 3). In addition to the association of paranodal terminal myelin loops with WSM, Schmidt-Lanterman incisures with WSM were also frequently observed (Figs. 8A, B; Table 3), but demyelination was not observed in these areas.

Tomacula were observed in both paranodal and internodal regions on longitudinal sections in all cases (Figs. 9A, B; Table 3). As in the transverse sections, almost all fibers with tomacula had WSM, especially in the outer layers of the myelin sheath (Figs. 9C, D). Large tomacula with complex redundant myelin loops in juxtaparanodal regions were also associated with widening of the node of Ranvier (i.e. demyelination).

Neurofilament densities in the axons in longitudinal sections were significantly greater in neuropathy versus normal control biopsies (number of filaments per micrometer, 13.9 ± 3.2 vs 9.8 ± 3.4 for paranode, $p < 0.01$; 12.7 ± 2.2 vs 9.0 ± 1.9 for juxtaparanode, $p < 0.05$; 10.2 ± 1.5 vs 7.5 ± 1.4 for internode, $p < 0.05$) (Fig. 10A). The increase in neurofilament density was most prominent in paranodal regions (Figs. 10A–C).
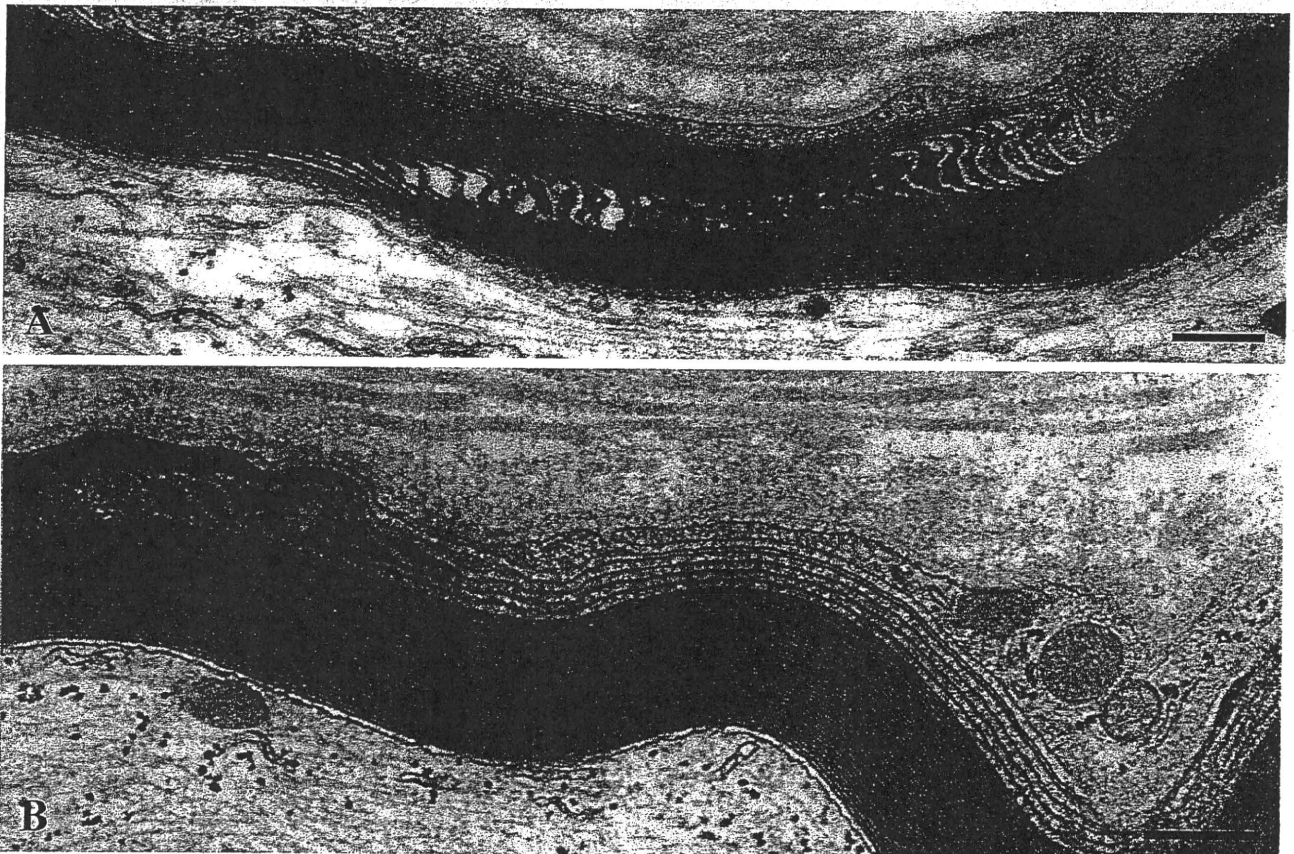

FIGURE 8. Electron micrographs of longitudinal sections of Schmidt-Lanterman incisures in specimens from a normal control (A) and anti–myelin-associated glycoprotein neuropathy (B). Widely spaced myelin is in continuity with Schmidt-Lanterman incisures. Scale bars = 0.5 μm.
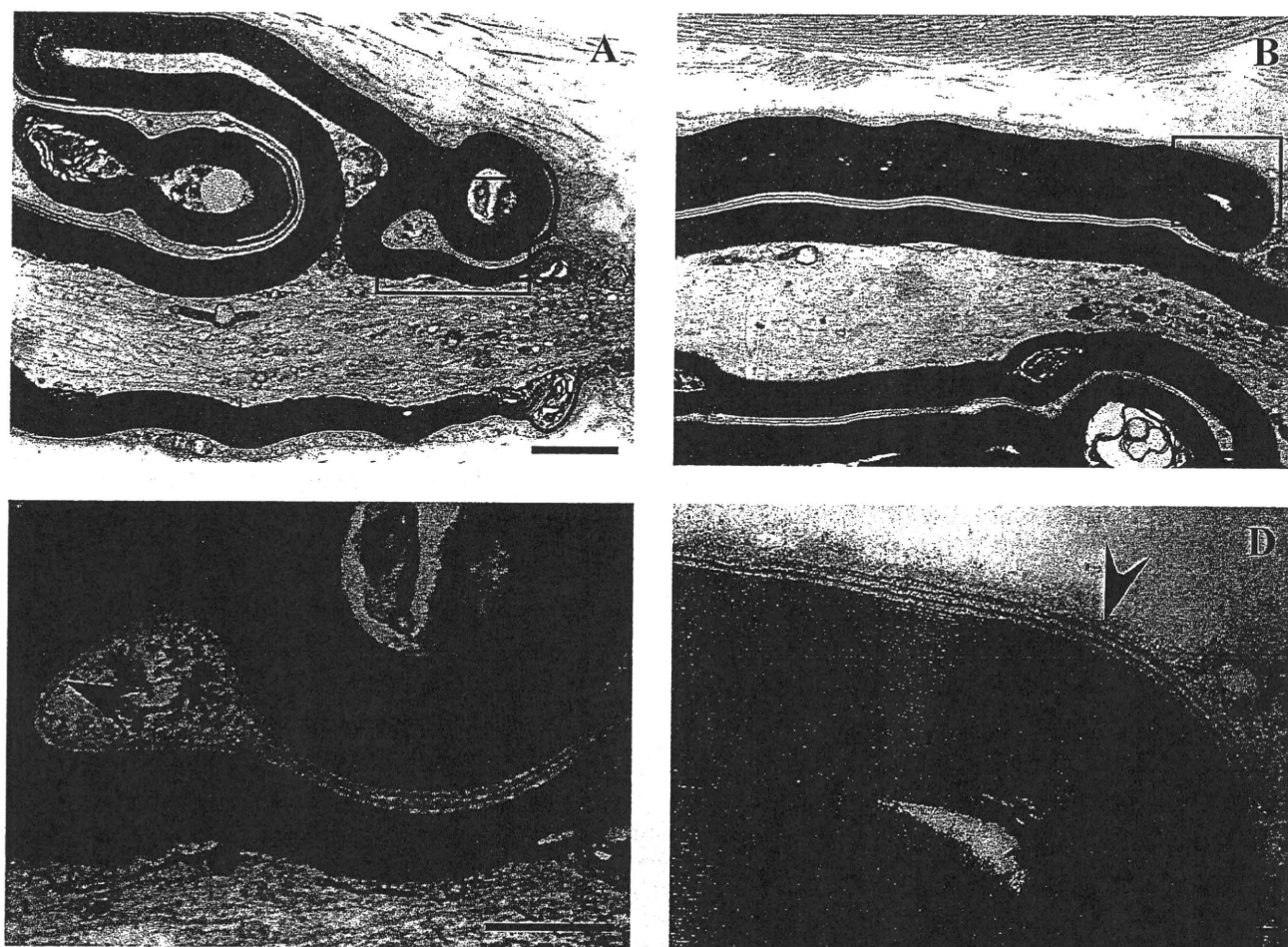
© *2010 American Association of Neuropathologists, Inc.*

1151

FIGURE 9. Electron micrograph of a longitudinal section at the paranodal and internodal regions showing tomaculous appearances. **(A, B)** Tomacula are observed in both paranodal **(A)** and internodal regions **(B)**. **(C, D)** High-power details of the boxed areas in **(A)** and **(B)** show widely spaced myelin in the outermost or some outer layers (arrowheads). Scale bars = **(A, B)** 1 μm; **(C, D)** 0.5 μm.

Immunofluorescence Staining

Indirect immunofluorescence was performed on cross sections and longitudinal sections in all cases. In cross sections, the MAG staining pattern was ringlike, corresponding to the periaxonal membrane, or double-line rings, corresponding to both the periaxonal membrane and Schmidt-Lanterman incisures. The IgM antibody deposits were present on both large and small myelinated nerve fibers (Fig. 11A). They appeared as either a thin line at the periphery of myelinated fibers or rings in the inner layer of the myelin sheath, corresponding to Schmidt-Lanterman incisures. In longitudinal sections, IgM deposits were continuous along the outermost layer of the myelin sheath and were concentrated at both paranodal regions and Schmidt-Lanterman incisures (Fig. 11B). These areas were consistent with those that showed WSM. No IgM deposit was seen on the periaxonal membrane on longitudinal sections. Immunoglobulin M and MAG were colocalized in paranodal regions and Schmidt-Lanterman incisures. Confocal microscopic analysis revealed colocalization of IgM and C3d (Figs. 11C–E), although C5b-9 (anti-TCC) was not observed on the myelin sheath.

DISCUSSION

Characteristic morphological changes in anti-MAG neuropathy include WSM, demyelination, axonal atrophy, and tomaculous appearance of myelinated fibers (15, 19, 20, 22, 23), and were found in all cases in our series. The pathogenic role of anti-MAG antibodies in this neuropathy has been investigated with passive immunization or systemic transfusion of anti-MAG IgM antibody into animals and was shown to cause WSM and myelin destruction (11, 35, 36). Immunoelectron microscopy demonstrated the selective presence of monoclonal IgM at the sites of myelin widening in patients with IgM monoclonal anti-MAG neuropathy (24). Thus, WSM is considered to be caused by direct binding of IgM to the myelin membrane, leading to abnormal myelin spacing (21, 37). However, it is still unclear how WSM develops morphologically and how its development correlates with the other characteristic findings in anti-MAG neuropathy. In this study, we demonstrated (*a*) a positive correlation between the frequency of WSM and demyelination and tomacula and the degree of reduction of myelinated fibers, (*b*) close association of WSM
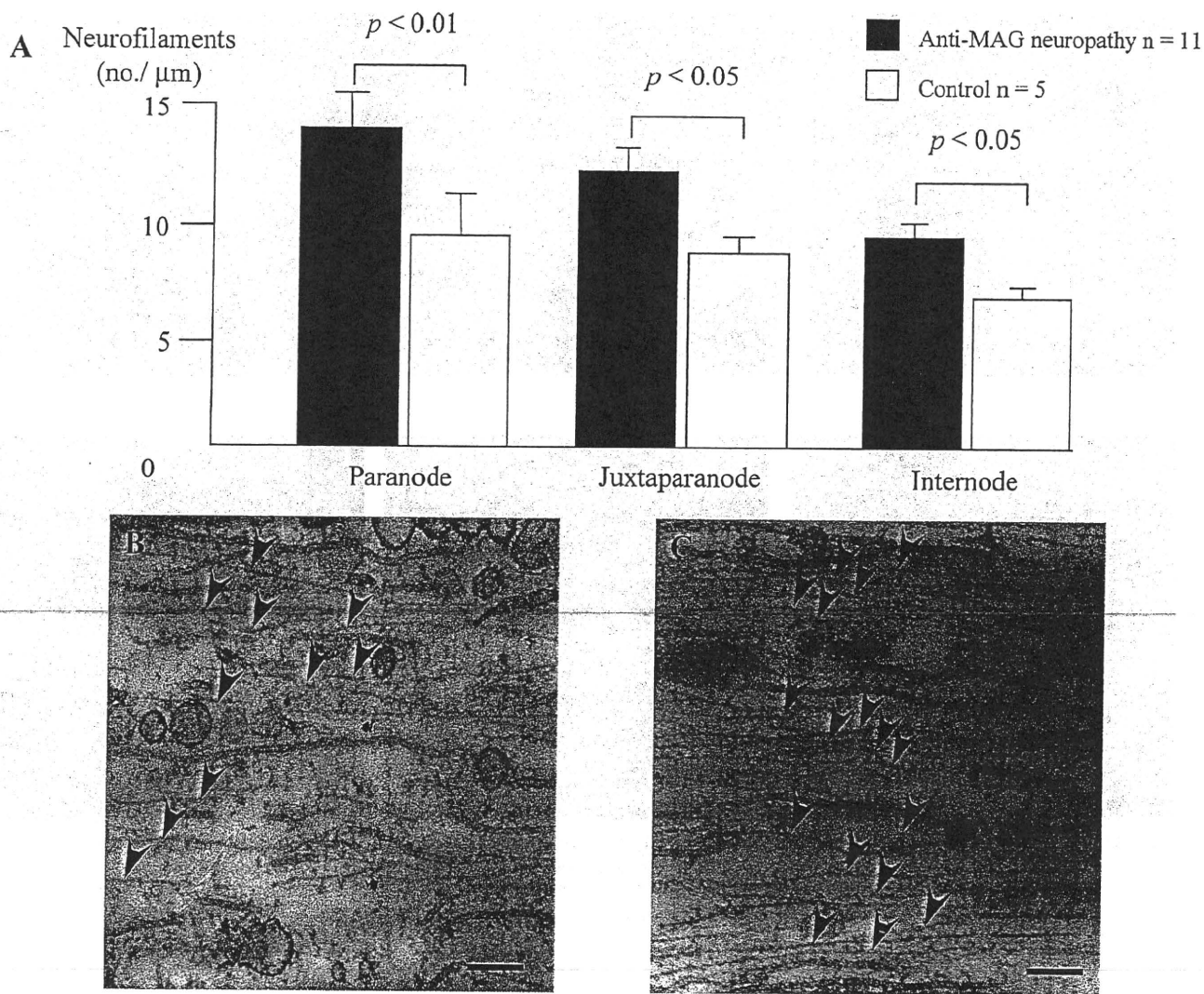
1152

FIGURE 10. Neurofilament density in longitudinal sections. **(A)** The number of neurofilaments is significantly greater in patients with anti–myelin-associated glycoprotein (MAG) neuropathy versus normal controls. **(B, C)** Electron micrographs of longitudinal sections of the paranodal region. The neurofilaments (arrowheads) in anti-MAG neuropathy **(C)** are denser than those in the normal control **(B)**. Scale bars = **(B, C)** 0.2 μm.

with redundant myelin loops with tomaculous appearance, (c) widening of the spaces between terminal myelin loops accompanied by their swelling as an early morphological change before demyelination, (d) the highest neurofilament density at paranodal regions, and (e) coincidence of areas with WSM and IgM deposition.

Our EM studies of longitudinal sections demonstrated that WSM developed in relation to the node of Ranvier, the outer layer of the myelin sheath, and Schmidt-Lanterman incisures. Immunofluorescence studies demonstrated positive staining of anti-IgM antibody in these areas. Previous studies have also reported that MAG is located on noncompact myelin such as paranodal loops and Schmidt-Lanterman incisures (38–40). The MAG plays a role in adhesion between Schwann cell membranes in paranodal regions and Schmidt-Lanterman

incisures; thus, dysfunction of the adhesive properties of MAG may lead to the unique morphological changes seen at those sites (41). In this context, the widening of the spaces between terminal myelin loops we observed may be one of the earliest changes that occur at the paranodal region. This widening may cause formation of WSM at paranodal regions and eventually lead to impairment of adhesion between myelin terminals and paranodal axolemma. Detachment of swollen terminal myelin loops from the paranodal axolemma may occur when widening occurs in the space between terminal myelin loops, and these morphological changes may be associated with demyelination at the node of Ranvier (Figs. 12A–E). The detachment may be further accelerated by loosening of myelin sheaths caused by WSM in the outer layer of the myelin sheath. Detachment of outer layers may enhance the retraction
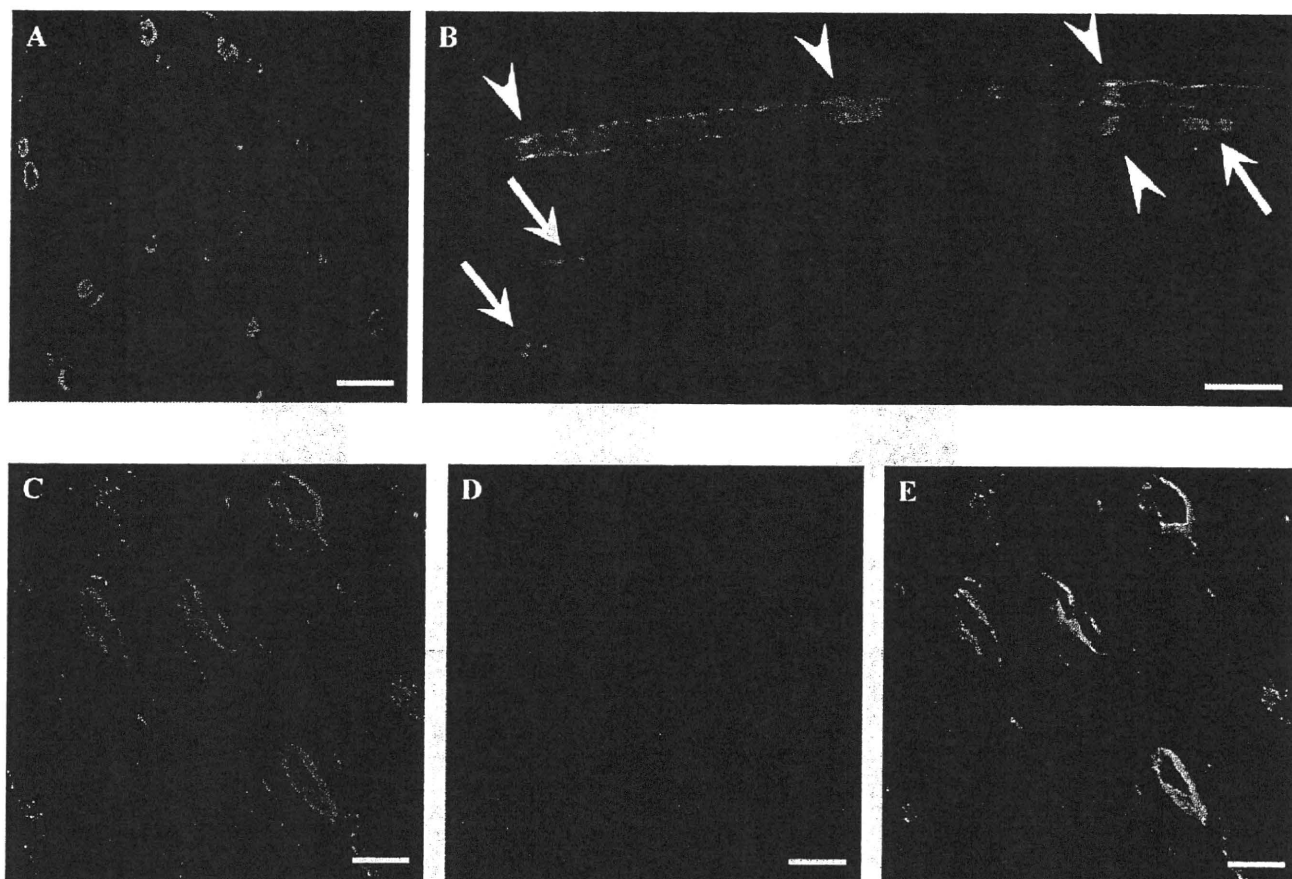
FIGURE 11. Immunofluorescence with anti-IgM antibody (green) on cross sections **(A)** and longitudinal sections **(B)** in anti-myelin-associated glycoprotein neuropathy. Immune reaction with the anti-IgM antibody is concentrated both in paranodal regions (arrows) and Schmidt-Lanterman incisures (arrowheads). Immunoglobulin M is also seen along the outermost layer of the myelin sheath. **(C–E)** Confocal microscopy reveals colocalization (yellow) in the merged image **(E)** of IgM (green) **(C)** and C3d (red) **(D)**. Scale bars = **(A, B)** 10 μm; **(C–E)** 3 μm.

of terminal myelin loops and lead to the widening of the node of Ranvier and subsequent demyelination. These observations were strongly supported by our immunohistochemical study and the correlation between the frequency of WSM and demyelination in teased fibers (Fig. 3). Furthermore, serum anti-MAG antibody titers were clearly correlated with the frequency of WSM in transverse sections and early pathological changes at the node of Ranvier. Together, our observations strongly suggest that anti-MAG antibodies induce WSM, other myelin changes, and subsequent demyelination and tomaculous formation.

In teased fibers and by EM, almost all tomacula with redundant myelin loops were accompanied by WSM. Because tomacula were found in both paranodal and internodal regions, loosening of myelin sheaths caused by WSM in the outer layer of the myelin sheath may be important in the formation of tomacula.

We confirmed the coexistence of both IgM and the complement component C3d, in paranodal regions and Schmidt-Lanterman incisures, as previously reported (42–45). Previous studies have suggested that the complement pathway, including the TCC, is the effector of myelin changes in neuropathy

associated with IgM monoclonal gammopathy (43) and experimental autoimmune neuritis (46). However, another study suggested that TCC may not be required for the breakdown of myelin components, or that the mechanism of IgM penetration into myelinated fibers through destruction of the basement membrane may not be mediated by TCC (45). We did not observe the TCC on myelin sheaths and, because of the slow progression in anti-MAG neuropathy that evolves during many years, the role of the complement pathway in anti-MAG neuropathy may be different from that in acute inflammatory demyelinating neuropathies in which TCC actively participates. Although active involvement of the complement pathway in the pathogenesis of anti-MAG neuropathy is still unclear, our finding that deposits of IgM and C3d were colocalized in the paranodal region suggests that the IgM antibody might injure myelin through activation of the complement pathway. Further investigation, including immunoelectron microscopy, may clarify the relationship between myelin alterations and the involvement of the complement pathway (24, 25, 47, 48).

In addition to paranodal loops and Schmidt-Lanterman incisures, MAG is also located on periaxonal membranes
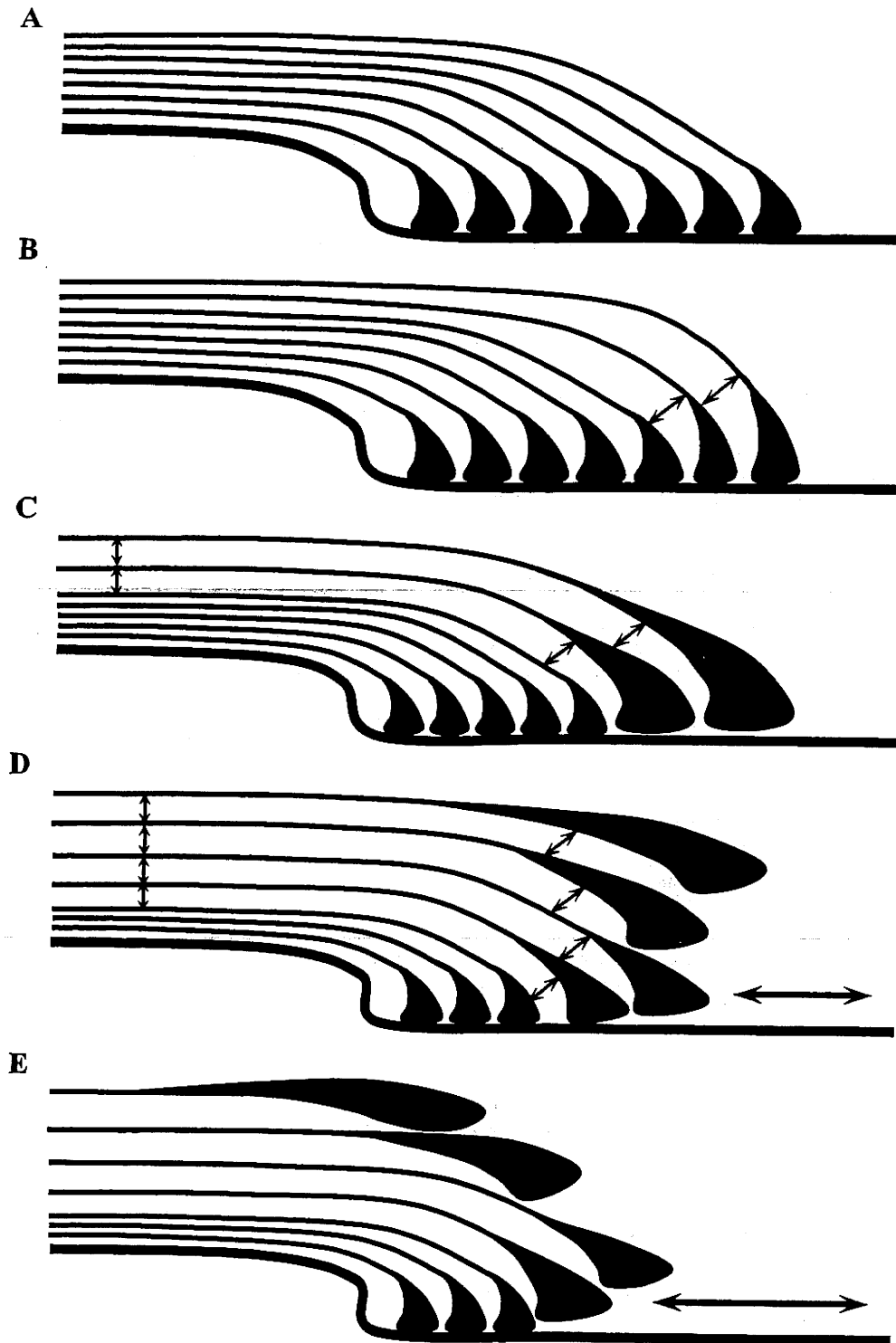
1154

FIGURE 12. Schematic representation of the progression of demyelination in anti–myelin-associated glycoprotein neuropathy. **(A)** Relationship between myelin terminals and paranodal axolemma in longitudinal sections of normal myelinated fibers. **(B)** Widening of spaces between myelin terminals. **(C)** Progression of the widening of spaces between terminal myelin loops with conspicuous swelling constitutes widely spaced myelin (WSM). **(D)** Some of these terminal myelin loops with conspicuous swelling are detached from the paranodal axolemma **(E)**. Detachment may be further accelerated by the loosening of myelin sheaths caused by WSM, leading to widening of the node of Ranvier.

1155

(38–40). The MAG in the periaxonal membrane plays a role in axon–Schwann cell signaling; the axon caliber of myelinated fibers in MAG-deficient mice is reduced because of decreased neurofilament phosphorylation (49–52). Consequently, dysfunction of MAG on the periaxonal side leads to an increase in neurofilament density and axonal atrophy, resulting in myelin collapse. However, we did not observe immunostaining for IgM or C3d in the periaxonal membrane, although MAG was located at that site. This finding might be caused by inaccessibility of the IgM antibody to the periaxonal membrane. We found that the neurofilament density was significantly increased in paranodes, juxtaparanodes, and internodes in anti-MAG neuropathy, with the highest density in the paranode. This suggests that axonal damage may be most severe in this region, and that axonal damage is initiated in paranodal regions where the initial stages of demyelination occur. Therefore, demyelination caused by detachment of terminal myelin loops from paranodal axolemma may be the primary cause of axonal atrophy and subsequent axonal damage in this neuropathy. Although the presence of MAG in unmyelinated fibers was not assessed, the preservation of unmyelinated fibers (in contrast to myelinated fibers) supports the view that demyelination is the primary cause of axonal damage in this neuropathy.

In summary, we demonstrated the close relationship between WSM and demyelination and tomacula. We suggest that the pathology occurring in myelin terminals in paranodal regions, which may be caused by activation of the complement pathway, results in extensive demyelination and subsequent axonal damage in anti-MAG neuropathy.

REFERENCES

1. Kelly JJ Jr. Peripheral neuropathies associated with monoclonal proteins: A clinical review. Muscle Nerve 1985;8:138–50
2. Hafler DA, Johnson D, Kelly JJ, et al. Monoclonal gammopathy and neuropathy: Myelin-associated glycoprotein reactivity and clinical characteristics. Neurology 1986;36:75–78
3. Steck AJ, Murray N, Dellagi K, et al. Peripheral neuropathy associated with monoclonal IgM autoantibody. Ann Neurol 1987;22:764–67
4. Latov N, Hays AP, Sherman WH. Peripheral neuropathy and anti-MAG antibodies. Crit Rev Neurobiol 1988;3:301–32
5. Smith IS. The natural history of chronic demyelinating neuropathy associated with benign IgM paraproteinaemia. A clinical and neurophysiological study. Brain 1994;117:949–57
6. Ellie E, Vital A, Steck A, et al. Neuropathy associated with "benign" anti-myelin-associated glycoprotein IgM gammopathy: Clinical, immunological, neurophysiological pathological findings and response to treatment in 33 cases. J Neurol 1996;243:34–43
7. Kuijf ML, Eurelings M, Tio-Gillen AP, et al. Detection of anti-MAG antibodies in polyneuropathy associated with IgM monoclonal gammopathy. Neurology 2009;73:688–95
8. Latov N. Pathogenesis and therapy of neuropathies associated with monoclonal gammopathies. Ann Neurol 1995;37:S32–S42
9. Steck AJ, Murray N, Justafre JC, et al. Passive transfer studies in demyelinating neuropathy with IgM monoclonal antibodies to myelin-associated glycoprotein. J Neurol Neurosurg Psychiatry 1985;48:927–29
10. Takatsu M, Hays AP, Latov N, et al. Immunofluorescence study of patients with neuropathy and IgM M proteins. Ann Neurol 1985;18:173–81
11. Tatum AH. Experimental paraprotein neuropathy, demyelination by passive transfer of human IgM anti-myelin-associated glycoprotein. Ann Neurol 1993;33:502–6
12. Vallat JM, De Mascarel HA, Bordessoule D, et al. Non-Hodgkin malignant lymphomas and peripheral neuropathies-13 cases. Brain 1995;118:1233–45
13. Nobile-Orazio E, Gallia F, Terenghi F, et al. How useful are anti-neural IgM antibodies in the diagnosis of chronic immune-mediated neuropathies? J Neurol Sci 2008;266:156–63
14. Stalder AK, Erne B, Reimann R, et al. Immunoglobulin M deposition in cutaneous nerves of anti-myelin-associated glycoprotein polyneuropathy patients correlates with axonal degeneration. J Neuropathol Exp Neurol 2009;68:148–58
15. Nobile-Orazio E, Francomano E, Daverio R, et al. Anti-myelin-associated glycoprotein IgM antibody titers in neuropathy associated with macroglobulinemia. Ann Neurol 1989;26:543–50
16. Rebai T, Mhiri C, Heine P, et al. Focal myelin thickenings in a peripheral neuropathy associated with IgM monoclonal gammopathy. Acta Neuropathol 1989;79:226–32
17. Gabriel JM, Erne B, Bernasconi L, et al. Confocal microscopic localization of anti-myelin-associated glycoprotein autoantibodies in a patient with peripheral neuropathy initially lacking a detectable IgM gammopathy. Acta Neuropathol 1998;95:540–46
18. Sander S, Ouvrier RA, McLeod JG, et al. Clinical syndromes associated with tomacula or myelin swellings in sural nerve biopsies. J Neurol Neurosurg Psychiatry 2000;68:483–88
19. Vital A, Lagueny A, Julien J, et al. Chronic inflammatory demyelinating polyneuropathy associated with dysglobulinemia: A peripheral nerve biopsy study in 18 cases. Acta Neuropathol 2000;100:63–68
20. Cai Z, Cash K, Swift J, et al. Focal myelin swellings and tomacula in anti-MAG IgM paraproteinaemic neuropathy: Novel teased nerve fiber studies. J Peripher Nerv Syst 2001;6:95–101
21. Melmed C, Frail D, Duncan I, et al. Peripheral neuropathy with IgM kappa monoclonal immunoglobulin directed against myelin-associated glycoprotein. Neurology 1983;33:1397–405
22. Vital A, Vital C, Julien J, et al. Polyneuropathy associated with IgM monoclonal gammopathy. Immunological and pathological study in 31 patients. Acta Neuropathol 1989;79:160–67
23. Jacobs JM, Scadding JW. Morphological changes in IgM paraproteinaemic neuropathy. Acta Neuropathol 1990;80:77–84
24. Lach B, Rippstein P, Atack D, et al. Immunoelectron microscopic localization of monoclonal IgM antibodies in gammopathy associated with peripheral demyelinative neuropathy. Acta Neuropathol 1993;85:298–307
25. Vallat JM, Vital A, Magy L, et al. An update on nerve biopsy. J Neuropathol Exp Neurol 2009;68:833–44
26. Nobile-Orazio E, Vietorisz T, Messito MJ, et al. Anti-MAG IgM antibodies in patients with neuropathy and IgM M proteins: Detection by ELISA. Neurology 1983;33:939–42
27. Sobue G, Hashizume Y, Mukai E, et al. X-linked recessive bulbospinal neuronopathy. A clinicopathological study. Brain 1989;112:209–32
28. Koike H, Iijima M, Sugiura M, et al. Alcoholic neuropathy is clinicopathologically distinct from thiamine-deficiency neuropathy. Ann Neurol 2003;54:19–29
29. Koike H, Iijima M, Mori K, et al. Neuropathic pain correlates with myelinated fibre loss and cytokine profile in POEMS syndrome. J Neurol Neurosurg Psychiatry 2008;79:1171–79
30. Dyck PJ, Giannini C, Lais A. Pathologic alterations of nerves. In: Dyck PJ, Thomas PK, Griffin JW, et al, eds. *Peripheral Neuropathy*, 3rd ed. Philadelphia, PA: WB Saunders, 1993:514–95
31. Koike H, Misu K, Sugiura M, et al. Pathology of early- vs late-onset TTR Met30 familial amyloid polyneuropathy. Neurology 2004;63:129–38
32. Koike H, Iijima M, Mori K, et al. Nonmyelinating Schwann cell involvement with well-preserved unmyelinated axons in Charcot-Marie-Tooth disease type 1A. J Neuropathol Exp Neurol 2007;66:1027–36
33. Ohnishi A, Hirano A. Uncompacted myelin lamellae in dysglobulinemic neuropathy. J Neurol Sci 1981;51:131–40
34. Verhagen WI, Gabreëls-Festen AA, van Wensen PJ, et al. Hereditary neuropathy with liability to pressure palsies: A clinical, electroneurophysiological and morphological study. J Neurol Sci 1993;116:176–84
35. Hays AP, Latov N, Takatsu M, et al. Experimental demyelination of nerve induced by serum of patients with neuropathy and an anti-MAG IgM M-protein. Neurology 1987;37:242–56
36. Monaco S, Ferrari S, Bonetti B, et al. Experimental induction of myelin changes by anti-MAG antibodies and terminal complement complex. J Neuropathol Exp Neurol 1995;54:96–104
37. Meier C, Vandevelde M, Steck A, et al. Demyelinating polyneuropathy associated with monoclonal IgM-paraproteinaemia. Histological, ultrastructural and immunocytochemical studies. J Neurol Sci 1984;63:353–67

38. Martini R, Carenini S. Formation and maintenance of the myelin sheath in the peripheral nerve: Roles of cell adhesion molecules and the gap junction protein connexin 32. Microsc Res Tech 1998;41:403–15

39. Trapp BD, Andrews SB, Wong A, et al. Co-localization of the myelin-associated glycoprotein and the microfilament components, F-actin and spectrin, in Schwann cells of myelinated nerve fibres. J Neurocytol 1989;18:47–60

40. Lopate G, Kornberg AJ, Yue J, et al. Anti–myelin-associated glyco-protein antibodies: Variability in patterns of IgM binding to peripheral nerve. J Neurol Sci 2001;188:67–72

41. Steck AJ, Stalder AK, Renaud S. Anti–myelin-associated glycoprotein neuropathy. Curr Opin Neurol 2006;19:458–63

42. Hays AP, Lee SS, Latov N. Immune reactive C3d on the surface of myelin sheaths in neuropathy. J Neuroimmunol 1988;18:231–44

43. Monaco S, Bonetti B, Ferrari S, et al. Complement-mediated demyeli-nation in patients with IgM monoclonal gammopathy and polyneurop-athy. N Engl J Med 1990;322:649–52

44. Ferrari S, Morbin M, Nobile-Orazio E, et al. Antisulfatide polyneurop-athy: Antibody-mediated complement attack on peripheral myelin. Acta Neuropathol 1998;96:569–74

45. Ritz MF, Erne B, Ferracin F, et al. Anti-MAG IgM penetration into

46. Stoll G, Schmidt B, Jander S, et al. Presence of the terminal complement complex (C5b-9) precedes myelin degradation in immune-mediated de-myelination of the rat peripheral nervous system. Ann Neurol 1991;30: 147–55

47. Vallat JM, Tabaraud F, Sindou P, et al. Myelin widenings and MGUS-IgA: An immunoelectron microscopic study. Ann Neurol 2000;47:808–11

48. Vallat JM, Magy L, Sindou P, et al. IgG neuropathy: An immunoelectron microscopic study. J Neuropathol Exp Neurol 2005;64:386–90

49. de Waegh SM, Lee VM, Brady ST. Local modulation of neurofilament phosphorylation, axonal caliber, and slow axonal transport by myelinat-ing Schwann cells. Cell 1992;68:451–63

50. Yin X, Crawford TO, Griffin JW, et al. Myelin-associated glycoprotein is a myelin signal that modulates the caliber of myelinated axons. J Neurosci 1998;18:1953–62

51. Lunn MP, Crawford TO, Hughes RA, et al. Anti–myelin-associated gly-coprotein antibodies alter neurofilament spacing. Brain 2002;125:904–11

52. Dashiell SM, Tanner SL, Pant HC, et al. Myelin-associated glycoprotein modulates expression and phosphorylation of neuronal cytoskeletal ele-ments and their associated kinases. J Neurochem 2002;81:1263–72

myelinated fibers correlates with the extent of myelin widening. Muscle Nerve 1999;22:1030–37

1157

IgM MGUS ANTI-MAG NEUROPATHY WITH PREDOMINANT MUSCLE WEAKNESS AND EXTENSIVE MUSCLE ATROPHY

YUICHI KAWAGASHIRA, MD,[1] NAOHIDE KONDO, MD,[1] NAOKI ATSUTA, MD, PhD,[1] MASAHIRO IIJIMA, MD, PhD,[1] HARUKI KOIKE, MD, PhD,[1] MASAHISA KATSUNO, MD, PhD,[1] FUMIAKI TANAKA, MD, PhD,[1] SUSUMU KUSUNOKI, MD, PhD,[2] and GEN SOBUE, MD, PhD[1]

[1] Department of Neurology, Nagoya University Graduate School of Medicine, Nagoya 466-8550, Japan
[2] Department of Neurology, Kinki University School of Medicine, Osaka, Japan

ABSTRACT: We report a patient with anti–myelin-associated glycoprotein (MAG) neuropathy, predominantly exhibiting severe motor symptoms, accompanied by extensive muscle atrophy mimicking Charcot–Marie–Tooth disease. Nerve conduction studies revealed mild retardation of motor conduction velocities and significant prolongation of distal latency. Sural nerve biopsy revealed widely spaced myelin and positive staining of myelinated fibers with an IgM antibody. Predominant motor symptoms with muscle atrophy can be one of the clinical manifestations of anti-MAG neuropathy.

Muscle Nerve 42: 433–435, 2010

Myelin-associated glycoprotein (MAG) is a minor component of the myelin membrane that plays an important role in axon–Schwann-cell interaction.[1–3] More than 50% of patients with neuropathy-associated IgM monoclonal gammopathy possess antibodies against MAG.[4]

Neuropathy associated with IgM monoclonal gammopathy of undetermined significance (MGUS) with an antibody against MAG represents a distinctive clinical syndrome characterized by male predominance, late age of onset, slow progression, predominantly sensory symptoms, and, in particular, the pronounced loss of deep sensation with sensory ataxia.[4–9] Conversely, predominant motor impairment has been reported only on occasion.[7,10] Herein, we report a patient with anti-MAG neuropathy presenting with predominantly motor symptoms and extensive muscle atrophy of the lower limbs, mimicking Charcot–Marie–Tooth (CMT) disease.

CASE REPORT

A 62-year-old man was admitted with distal muscle weakness of the lower limbs, which was accompanied by marked muscle atrophy. He did not have a notable individual or family history, and there were no growth problems during his infancy. Muscle weakness of the bilateral toes began approximately 5 years prior to our clinical evaluation, along with slow progression in the bilateral lower limbs. Muscle atrophy of the lower limbs gradually became conspicuous. In addition, mild paresthesia in the distal portion of the lower limbs developed over the last 2 years. On admission, neurological examination revealed bilateral severe muscle weakness and extensive muscle atrophy, predominantly in the distal portion of the legs (Fig. 1A). Manual muscle testing, recorded in the lower legs, was level 1. Neither muscle weakness nor muscle atrophy was observed in the upper extremities. Touch, pain, vibratory, and joint sensations of all extremities were mildly reduced in a glove-and-stocking distribution Pseudoathetosis was not observed in the hand. A Romberg sign could not be determined because the patient could not remain standing unaided. There were no abnormalities in the cranial nerves and autonomic nervous system. Deep tendon reflexes were absent on both sides of the legs and arms.

In routine laboratory examinations, we found that the serum IgM level was significantly elevated to 890 mg/dl (normal 35–220 mg/dl), and IgM-kappa–type M-protein was identified by serum immune electrophoresis. Western blotting confirmed positive serum anti-MAG IgM antibody. In addition, sulfoglucuronyl paragloboside (SGPG) IgM antibody titer was also significantly elevated, based on the results of an enzyme-linked immunosorbent assay. In contrast, serum IgM and IgG antibodies to GM1, GM2, GM3, GD1a, GD1b, GD3, GT1b, GQ1b, GA1, Gal-c were all negative.[11] Analysis of cerebrospinal fluid showed that protein content was increased significantly at 380 mg/dl (normal range 15–45 mg/dl), whereas cell count was normal. The ratio of plasma cells in the bone marrow was less than 5%, and no lymphoplasmacytoid elements were evident.

Motor nerve conduction studies in the median and ulnar nerve revealed mild retardation of 42 m/s and 43 m/s, respectively. Significant prolongations of distal latency in the median and ulnar nerve were highly conspicuous, at 13.2 ms and 5.7 ms, respectively. Compound muscle action potential amplitudes in the median and ulnar nerve were 4.4 mV and 5.8 mV, respectively. Motor and sensory
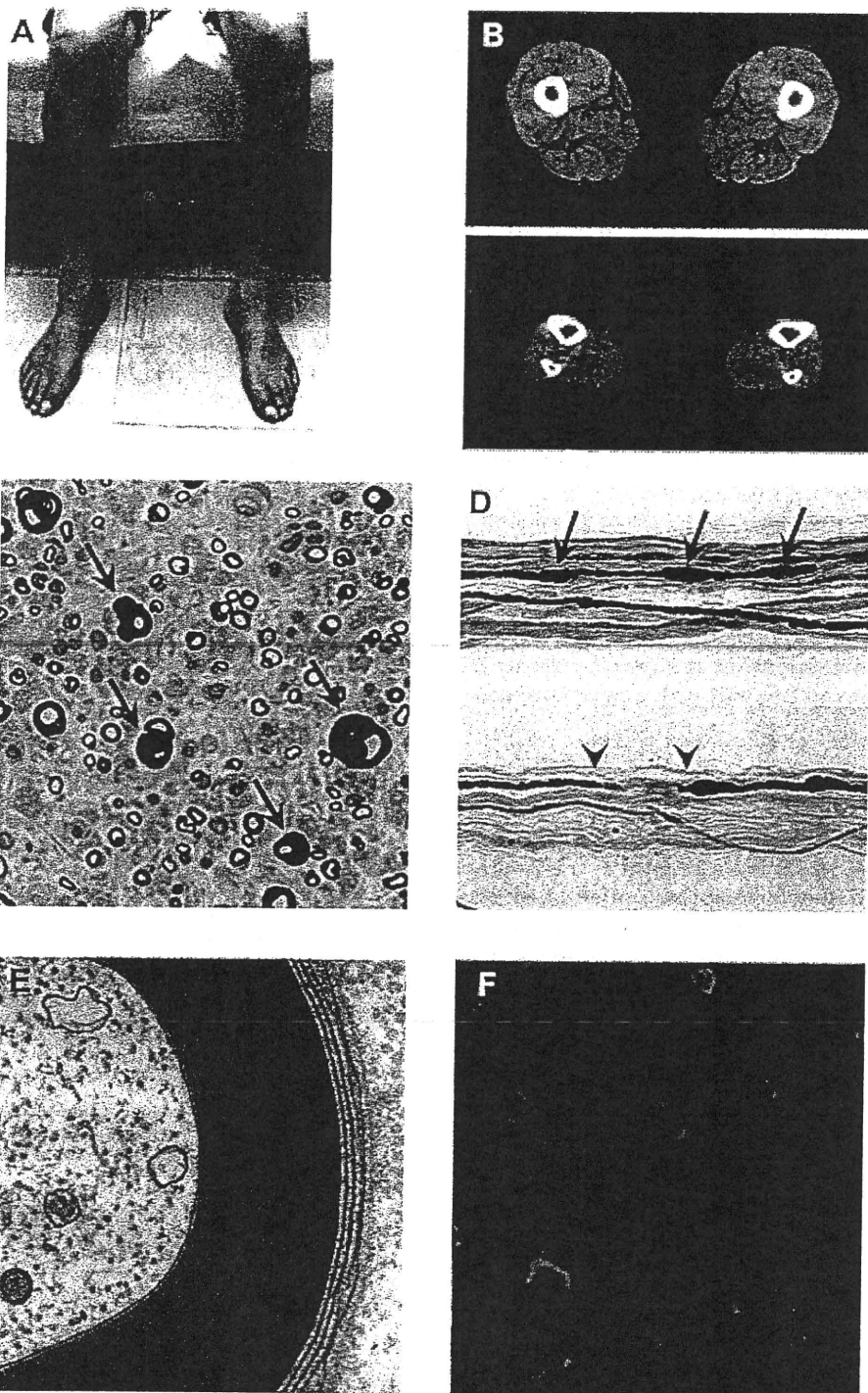
FIGURE 1. (A) The patient's lower extremities. Bilateral lower legs are visibly atrophic. (B) Muscle computed tomography of the lower extremities. Muscle atrophy predominant in the lower legs (lower panel) is evident. (C) Transverse section of a sural nerve biopsy stained with toluidine blue. Fibers with redundant myelin loops are observed (arrows). (D) Teased fibers show tomacula (arrows) and segmental demyelination (arrowheads). (E) Electron micrographs of the transverse section. Widely spaced myelin is observed in some outer lamellae of the myelin sheath. (F) Immunofluorescence study of cross-sections. The immune reaction with IgM antibody is positive on the myelin sheath. [Color figure can be viewed in the online issue, which is available at www.interscience.wiley.com.]

nerve conduction studies in the lower limbs and sensory nerve conduction studies in the upper limbs were not elicited at all. Magnetic resonance imaging (MRI) suggesting spinal disorders was not seen in the spinal cord and the cauda equina was not enhanced with gadolinium. Computed